Quasifission barrier of heavy ion fusion reactions leading to the formation of the superheavy nucleus $^{302}120$

P. S. Damodara Gupta,[1,2] N. Sowmya [ORCID],[1,*] H. C. Manjunatha,[1,†] L. Seenappa [ORCID],[1] and T. Ganesh [ORCID][2]

[1]*Department of Physics, Government College for Women, Kolar 563101, Karnataka, India*
[2]*Department of Physics, Rajah Serfoji Government College, Thanjavur 613005, Tiruchirappalli, Tamil Nadu, India*
affiliated to Bharathidasan University, Tiruchirappalli, Tamil Nadu, India

We study the quasifission barriers of different fusion reactions leading to synthesis of the superheavy element $Z = 120$ using the dinuclear system approach. In particular, the influence of the projectile-target orientation and angular momentum on quasifission barriers has been investigated. The quasifission barrier height is observed to be maximum when the angle of orientation of projectile-target is about $90°$ (tip-tip orientation). The role of entrance channel effects on quasifission barriers is investigated, and also suggested are suitable empirical formulas for the same. The striking results leading to larger quasifission barriers, whose cross sections are >10 fb, are also mentioned. As a result, the current research might be valuable in developing corrective techniques for future experimental attempts to synthesize superheavy nuclei with $Z = 120$.

I. INTRODUCTION

The competing quasifission process greatly hampers the synthesis of superheavy elements (SHEs) by the fusion of two massive nuclei; i.e., it hinders the heavy ion fusion by breaking into two fragments within zeptoseconds. The formation of compound nuclei is a structural dependence of both the projectile and target nuclei. As a result, quasifission causes fusion hindrance during the formation of heavy nuclei [1]. It is also evident from the literature [2,3] that "side-side" collisions lead mainly to fusion-fission whereas "tip-tip" collisions lead to a quasifissionprocess. The dynamics of heavy ion collisions show that complete fusion does not occur near Coulomb barrier energies [4–6]. The fission of a dinuclear configuration that does not result in the production of a compound nucleus is known as quasifission. It spans the gap between deep-inelastic collisions, in which the reaction partners collide and exchange numerous particles without affecting their average mass and charge. When the compound nucleus is produced, the reaction partners lose their identities in the fusion process.

The superheavy elements with atomic number $Z \geqslant$ Rf are not abundant in nature. These elements were synthesized using cold and hot fusion reactions. The cold fusion reactions are associated lead and bismuth targets with low excitation energy (10 to 20 MeV) [7,8]. However, hot fusion reactions involve ^{48}Ca projectiles on actinide targets [9–11]. Many fusion reactions were attempted after the synthesis of SHE oganesson. Reactions such as ^{54}Sc + ^{249}Cf, ^{50}Ti + ^{249}Bk, ^{51}V + ^{248}Cm, ^{54}Cr + ^{243}Am, ^{55}Mn + ^{244}Pu, ^{58}Fe + ^{237}Np, and ^{59}Co + ^{238}U were experimentally attempted in order to synthesize the superheavy element $Z = 119$ [12,13]. Sim-ilarly, many theoretical studies focus on the prediction of superheavy element $Z = 119$ [14–19] using the dinuclear system (DNS), an advanced statistical model, the dinuclear system model with a dynamical potential energy surface, and modified diffusion models. Similarly, experimental and theoretical attempts were carried out to synthesize the superheavy element $Z = 120$ using different projectile-target combinations such as ^{50}Ti + ^{249}Cf, ^{51}V + ^{249}Bk, ^{54}Cr + ^{248}Cm, ^{55}Mn + ^{243}Am, ^{58}Fe + ^{244}Pu, ^{59}Co + ^{237}Np, and ^{64}Ni + ^{238}U [12,13,20–22].

The formation of superheavy nuclei requires a precise balancing act. On one side, low E_x reduces fission competition, which may be achieved by utilizing heavier projectiles. On the other hand, by reducing the charge product of the two colliding nuclei, quasifission should be minimized (and therefore P_{CN} maximized) [23]. It is hard to see the difference between fission events from fused compound nuclei and so-called quasifission events from a dinuclear system within experiments. As a result, quantitative comparisons with theoretical estimates may not be possible using experimental fusion cross sections. Full momentum transfer was observed for the fusion reaction ^{30}Si + ^{238}U at bombardment energies near the Coulomb barrier [24].

The analysis shows that mass distributions were Gaussian with mass symmetry at energies above the Bass barrier. At sub-barrier energies, an asymmetric fission channel is observed, implying competition between fusion and quasifission based on the evaporation residue (ER) cross section produced in the fusion reaction ^{30}Si + ^{238}U. This suggests that quasifission is also responsible for the asymmetric channel [24]. The experimental measurement of the fragments' mass-angle correlations in ^{40}Ca + ^{238}U was combined with microscopic quantum computations. An unanticipated interaction is observed between the prolate deformed ^{238}U orientation and quantum shell effects in the fragments. Interpretations reveal

*Corresponding author: sowmyaprakash8@gmail.com
†Corresponding author: manjunathhc@rediffmail.com

that only collisions with the tip of ^{238}U yield quasifission fragments in the magical area ($Z = 82$), whereas collisions with the side result in fusion [25]. Experimental results have demonstrated that if the beam energy is reduced from above-barrier to sub-barrier levels, a change from symmetric to asymmetric mass distributions is observed [26]. The production cross sections were predicted using different projectiles with actinide targets by considering the role of entrance channel parameters [27–35].

Adamian *et al.* [36] evaluated mean-field potentials using HFB calculations and also predicted production cross sections in the superheavy element region from Cn to $Z = 120$. Previous researchers [37] predicted production cross sections for superheavy nuclei from 119 to 122 by including orientation effects using a Monte Carlo–assisted DNS model. The production cross section for the fusion reaction ^{54}Cr + ^{243}Am leading to formation of superheavy nuclei $Z = 119$ was studied using KEWPIE statistical code and the DNS model [38]. Adamian *et al.* [39] studied fusion reactions such as ^{50}Ti + ^{249}Bk and ^{51}V + ^{248}Cm for the formation of superheavy nuclei $Z = 119$ using the DNS model. Adamian and Antonenko [40] predicted optimal reactions to synthesize superheavy elements $Z = 119$ and 120. The fusion-evaporation and multinucleon transfer (MNT) approaches were included in the investigation of fusion reactions such as ^{48}Ca + ^{238}U within the DNS model [41]. Apart from the above results, some other researchers also studied fusion reactions to synthesize superheavy nuclei using the DNS model [42–44].

Hence in this article we study the role of the angle of orientation of the projectile-target combination, deformations, entrance channel parameters such as the Coulomb interaction parameter, mean fissility, charge asymmetry, mass asymmetry, isospin asymmetry, and charge product. As a result, we thus focus on the hindrance of the formation of superheavy elements by the study of quasifission barriers on different projectile-target combinations. The present paper is organized as follows; The evaluation of the quasifission barrier and angle of orientation on different projectile-target combinations and the role of entrance channel effects on the projectile-target combinations are presented in Sec. II. A detailed analysis of the present work is furnished in Sec. III. The conclusions drawn from the present work are given in Sec. IV.

II. THEORETICAL FRAMEWORK

Within the dinuclear system model, the quasifission barrier $B_{qf}(Z, A, \ell, \alpha_i)$ [45] is expressed as

$$B_{qf}(Z, A, l) = V(R_b, Z, A, \beta_{21}, \beta_{22}, l, \alpha_i)$$
$$- V(R_m, Z, A, \beta_{21}, \beta_{22}, l, \alpha_i). \quad (1)$$

Here ℓ is the angular momentum, and the nucleus-nucleus potential is minimum at distance $R = R_m$ and it is evaluated as explained in detail in the literature [45]. Over the quasifission barrier, the local temperature of the dinuclear system is given by

$$\Theta_{DNS}(Z, A) = \sqrt{\left(\frac{E_{DNS} - B_{qf}}{a} \right)}. \quad (2)$$
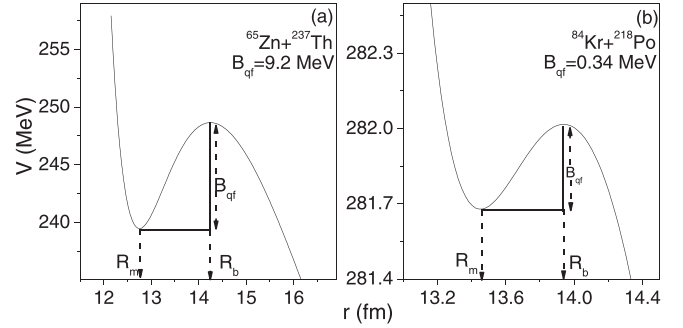
FIG. 1. (a) A plot of the nucleus-nucleus interaction potential using the DNS approach for the fusion reactions ^{65}Zn + ^{237}Th and (b) ^{84}Kr + ^{218}Po which lead to compound nucleus ^{302}120, as a function of separation distance R between centers of DNS fragments.

The $E_{DNS} = E_{cm} - V(R_m)$ is the excitation energy of the dinuclear system and E_{cm} is the center-of-mass energy. The nucleus-nucleus interaction potential of the dinuclear system is given by

$$V(R, Z_1, Z_2, \beta_{2i}, l, \alpha_i)$$
$$= V_c(R, Z_1, Z_2, \beta_{2i}, \alpha_i)$$
$$+ V_N(R, Z_1, Z_2, \beta_{2i}, \alpha_i) + V_{rot}(l, \beta_{2i}). \quad (3)$$

Here Coulomb, nuclear, and rotational potentials are denoted by V_C, V_N, and V_{rot}, and they are evaluated as explained in the Refs. [45,46]. The driving potential is evaluated as

$$U(Z, A, R, \alpha_i) = V(R, Z_1, Z_2, \beta_{2i}, l, \alpha_i) - Q, \quad (4)$$

and Q is the mass excess energy given by

$$Q = B_1(Z_1) + B_2(Z_2) - B_{CN}(Z_{CN}), \quad (5)$$

where $B_1(Z_1)$ and $B_2(Z_2)$ are the binding energies of the fragments in the DNS at their ground states and $B_{CN}(Z_{CN})$ is the binding energy of the compound nucleus; they are taken from [47].

III. RESULTS AND DISCUSSIONS

Around 90 different projectile-target combinations were analyzed for the synthesis of superheavy element ^{302}120. Using DNS approach, quasifission barriers of all these different projectile-target combinations were evaluated as explained in the theory section. The role of the angle of orientation of the projectile-target combination was involved in the evaluation of Coulomb potential [45,46]. The nucleus-nucleus potential evaluated for the fusion reactions ^{65}Zn + ^{237}Th and ^{84}Kr + ^{218}Po as a function of separation distance R between centers of DNS fragments is depicted in Fig. 1. The term $R_m = 12.75$ fm is the distance at which the potential is found to be minimum and $R_b = 14.25$ fm is the distance at which the potential is maximum for the fusion reaction ^{65}Zn + ^{237}Th. The mass and charge asymmetries for the fusion reaction ^{65}Zn + ^{237}Th are about 0.57 and 0.75 respectively. The quasifission barrier for ^{65}Zn + ^{237}Th is found to be 9.2 MeV, as seen in Fig. 1(a). Similarly, for the fusion reaction ^{84}Kr + ^{218}Po the turning points are found to be $R_m = 13.44$ fm
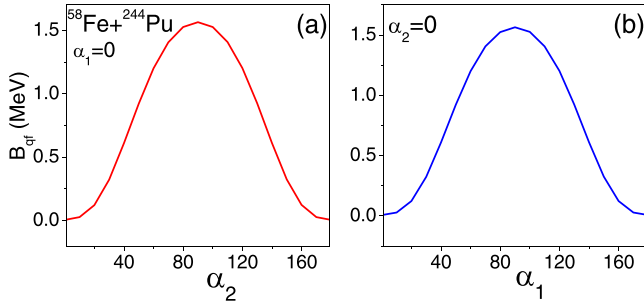
FIG. 2. (a) Variation of the quasifission barrier (B_{qf}) as function of target orientation angle (α_2), keeping the projectile orientation angle at zero ($\alpha_1 = 0$). (b) Variation of quasifission barrier (B_{qf}) as function of projectile orientation angle (α_1), keeping the target orientation angle at zero ($\alpha_2 = 0$).

and $R_B = 13.94$ fm and the quasifission barrier has been established as $B_{qf} = 0.34$ MeV, which is clearly shown in Fig. 1(b). The mass and charge asymmetries of the fusion reaction ^{84}Kr + ^{218}Po are 0.53 and 0.7 respectively. Hence, detailed analysis shows that the quasifission barrier is larger for ^{65}Zn + ^{237}Th when compared to ^{84}Kr + ^{218}Po. A thorough examination shows that the quasifission barrier is larger when mass and charge asymmetries are found to be maximum, as seen in the case of ^{65}Zn + ^{237}Th when compared to ^{84}Kr + ^{218}Po. Accordingly, when the quasifission barriers are maximum then the probability of the formation of compound nuclei will be more. In addition to mass and charge asymmetries, the orientation angle also plays a major role in the formation of superheavy elements. Larger values of quasifission barrier are analyzed by keeping the projectile orientation angle at zero ($\alpha_1 = 0$) and varying the target orientation angle, as seen in Fig. 2(a). The quasifission barrier increases with respect to the angle of orientation of the target nuclei, and reaches a maximum value when $\alpha_2 = 90°$, and then the quasifission barrier decreases with an increase in the target's orientation angle. Similar results were also observed when the target orientation angle was kept at zero ($\alpha_1 = 0$) by varying the projectile's orientation angle [see Fig. 2(b)]. Hence, it is inferred from both the figures that the quasifission barriers are maximum when the projectile's and target's angle of orientation is $\alpha_1/\alpha_2 = 90°$. In the latter case, we simultaneously varied projectile's and target's angle of orientation as specified in Fig. 3. The orange and yellow color specifies projectile and target orientation angles. The angle of orientation varies between 0° and 90°. The maximum value of the quasifission barrier is observed when the collision between a projectile-target combination is found to be 90°-90°, i.e., for tip-tip collisions, and B_{qf} is minimum when the angle of orientation is 0°-0°, i.e., for side-side collisions.

A. Deformation and entrance channel effects on projectile-target combinations

In the synthesis of compound nuclei, entrance channel parameters such as Coulomb interaction parameter ($z = \frac{Z_1 Z_2}{A_1^{1/3} + A_2^{1/3}}$), mean fissility ($\chi_m = 0.25\chi_{CN} + 0.75\chi_{eff}$), mass
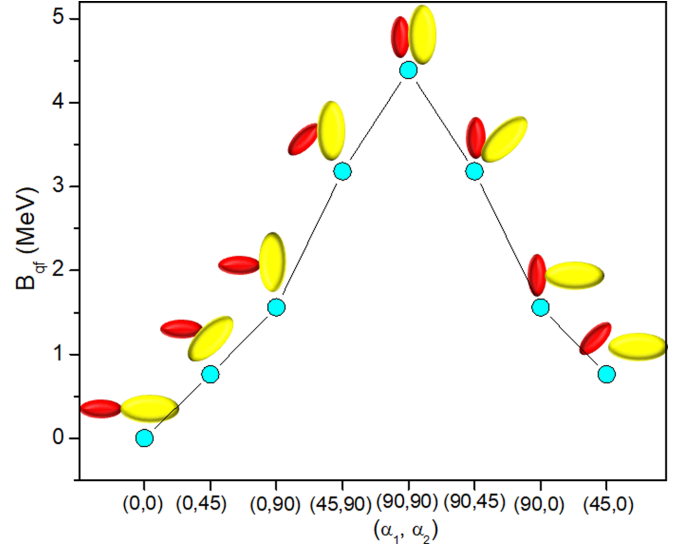
FIG. 3. Variation of quasifission barrier (B_{qf}) as function of varying projectile and target orientation angle.

asymmetry ($\eta_A = \frac{A_1 - A_2}{A_1 + A_2}$), charge asymmetry ($\alpha_z = \frac{Z_1 - Z_2}{Z_1 + Z_2}$), isospin asymmetry [$\Delta(N/Z)$], and charge product ($Z_1 Z_2$) play a significant role [34]. A systematic analysis of the quasifission barrier using different projectile-target combinations and entrance channel parameters is carried out. The literature also shows that deformations of the projectile and target play a key role in the production of compound nuclei [34,48–50]. Hence, in the present investigations, we have considered three cases, in which projectile-target combinations were categorized as (a) oblate projectile ($\beta_{2P} < 0$) and prolate target ($\beta_{2T} > 0$), (b) prolate projectile and target ($\beta_{2P} > 0, \beta_{2T} > 0$) nuclei, and (c) spherical projectile ($\beta_{2P} = 0$) and prolate target ($\beta_{2T} > 0$). Since we have investigated all possible combinations of projectile and target, we have not identified any target other than prolate. But for the projectile, we noticed all the three cases $\beta < 0$, $\beta = 0$, and $\beta > 0$. For the first case, we have identified 25 projectile-target combinations with $\beta_{2P} < 0$, $\beta_{2T} > 0$. Further, we noticed a maximum of 50 projectile-target combinations with $\beta_{2P} > 0$, $\beta_{2T} > 0$, and in the third case around 15 projectile-target combinations are recognized with $\beta_{2P} = 0$, $\beta_{2T} > 0$.

1. Case I: $\beta_{2P} < 0$ and $\beta_{2T} > 0$

Figure 4 shows the variation of B_{qf} as a function of entrance channel parameters for the projectile-target combinations with $\beta_{2P} < 0$, $\beta_{2T} > 0$. Figure 4(a) shows a plot of the quasifission barrier as a function of the Coulomb interaction parameter (z). The value of B_{qf} increases with an increase in z. Since there is a systematic variation of B_{qf} as a function of z, we tried to fit empirical formulas for the same. We tried many functions such as $B_1 z + B_2 z^2 + B_3$, $B_1 z + B_2 z/(z - B_3)$, $B_1 \ln(z - B_2) + B_3$, $B_1 z + B_2 + B_3/z$, $B_1 \exp^{B_2} /[z - B_3 \ln(z)]$, $z^{B_1} \exp^{B_2 - B_3}$, $B_1 \ln(z) + B_2$, $\frac{1}{B_1 \ln(z) + B_2}$, and also the polynomial function $B_0 + B_1 z + B_2 z^2 + B_3 z^3 + B_4 z^4$. Here B_1, B_2, B_3, and B_4 are the fitting constants. Among the functions analyzed, we chose an
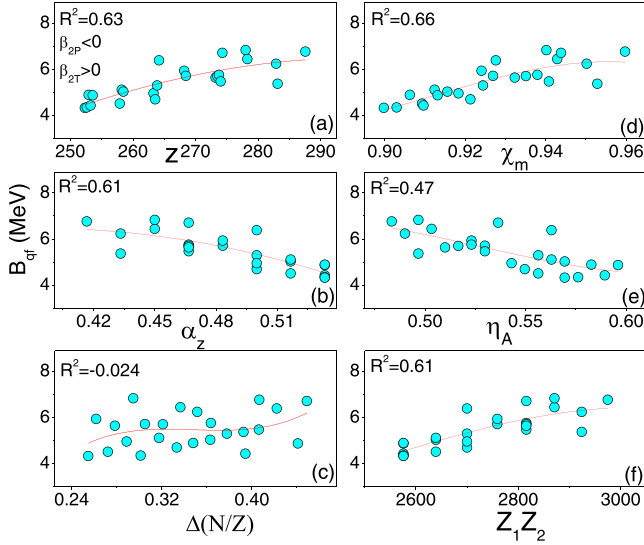
FIG. 4. Variation of quasifission barrier (B_{qf}) for tip-tip collision as function of (a) Coulomb interaction parameter, (b) mean fissility, (c) charge asymmetry, (d) mass asymmetry, (d) isospin asymmetry, and (e) charge product when the projectile is oblate ($\beta_{2P} < 0$) and the target is prolate ($\beta_{2T} > 0$).

equation that maximizes the coefficient of determination (R^2) and minimizes the residual sum of squares (RSS). Among the studied equations, we have considered the third-order polynomial equation whose residual sum of squares is nearly equal to 1. Finally, the constructed equation for B_{qf} as a function of z is

$$B_{qf} = \sum_{i=0}^{3} \delta_i x^i, \tag{6}$$

where the value of δ_i is the fitting constant, i.e., i varies between 0 to 3, and x corresponds to the Coulomb interaction parameter (z). Similarly, we have observed an increase in B_{qf} as a function of χ_m and $Z_1 Z_2$ as seen in Figs. 4(d) and 4(f). Furthermore, B_{qf} decreases with increase in α_z and η_A [Figs. 4(b) and 4(e)]. However, no systematic variation is observed in the case of isospin asymmetry shown in Fig. 4(c). A detailed analysis of the figure shows a larger coefficient of determination when $R^2 = 0.66$ in the case of B_{qf} as a function of χ_m. A suitable function used to fit the quasifission barrier as a function of χ_m is given by Eq. (6) where $x = \chi_m$. The coefficients of fitting constants which vary between $i = 0$ and 3 are tabulated in Table I.

2. Case II: $\beta_{2P} > 0$ and $\beta_{2T} > 0$

Second, we have considered the case of projectile and target being prolate ($\beta_{2P,2T} > 0$), in which the quasifission barriers are studied as a function of entrance channel parameters as seen in Fig. 5. In this case, we have observed a decrease in quasifission barriers with respect to z, χ_m, and charge product $Z_1 Z_2$ as seen in Figs. 5(a), 5(b), and 5(f). On the other hand, the quasifission barrier increases with charge and mass asymmetry as seen in Figs. 5(b) and 5(e)

TABLE I. Tabulation of fitting constants of quasifission barrier as a function of χ_m and z.

TOR	Parameter	δ_0	δ_1	δ_2	δ_3
$\beta_{2P} < 0$					
	χ_m	6690.82	$-22\,106.4$	24 307.18	-8888.36
$\beta_{2T} > 0$					
$\beta_{2P} > 0$					
	z	-76.29	1.0034	-0.0039	4.69×10^{-6}
$\beta_{2T} > 0$					
$\beta_{2P} = 0$					
	χ_m	1936.72	-6468.88	7253.61	-2724.69
$\beta_{2T} > 0$					

respectively. Similarly to the earlier case, here we have not observed any systematic variation of B_{qf} as a function of isospin asymmetry [see Fig. 5(c)]. The detailed investigations show a larger coefficient of determination when $R^2 = 0.989$ for B_{qf} as a function of z. A suitable function used to fit the quasifission barrier as a function of z is given in Eq. (6) where $x = z$. The coefficients are tabulated in Table I.

3. Case III: $\beta_{2P} = 0$ and $\beta_{2T} > 0$

Finally, we have considered the case in which the projectile is spherical ($\beta_{2P} = 0$) and the target is prolate ($\beta_{2P} > 0$) as seen in Figs. 6(a)–(f). Here also we have observed a decrease in B_{qf} with respect to z, χ_m, $\Delta(N/Z)$, and $Z_1 Z_2$, which is shown in Figs. 6(a), 6(b), 6(c), and 6(f). In contrast, the increment of B_{qf} is observed with respect to α_z and η_A as seen in Figs. 6(b) and 6(e). Further analysis reveals a higher coefficient of determination ($R^2 = 0.99$) for B_{qf} as a function of χ_m. The appropriate function for fitting the quasifission
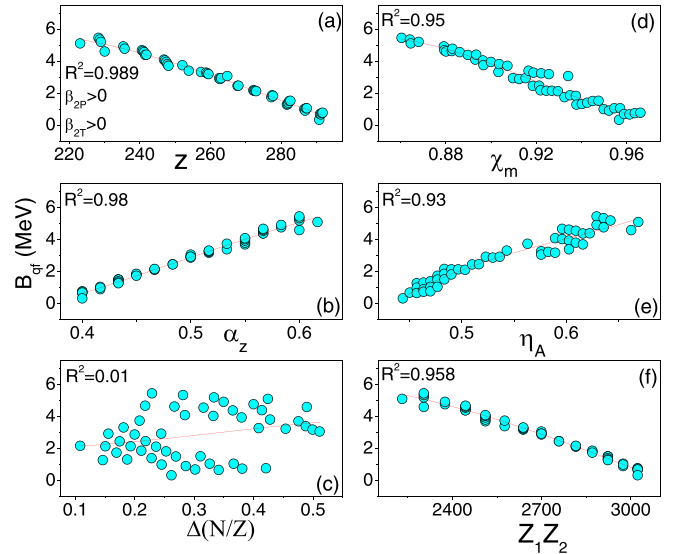
FIG. 5. Variation of quasifission barrier (B_{qf}) for tip-tip collision as function of (a) Coulomb interaction parameter, (b) mean fissility, (c) charge asymmetry, (d) mass asymmetry, (d) isospin asymmetry, and (e) charge product when the projectile and target are prolate ($\beta_{2P,2T} > 0$).
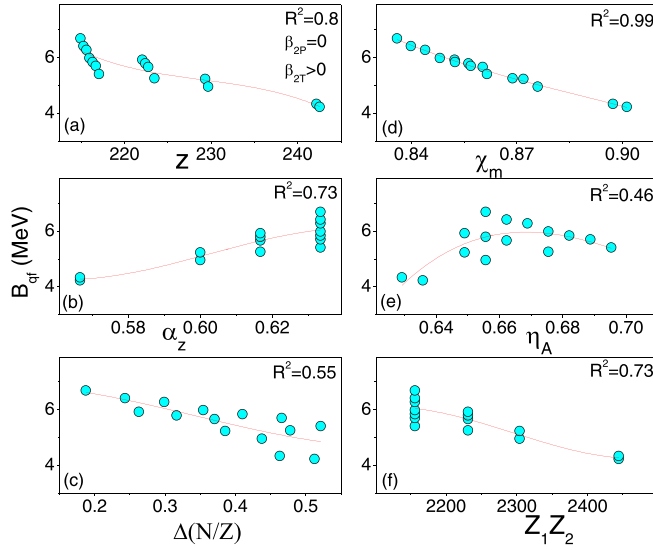
FIG. 6. Variation of quasifission barrier (B_{qf}) for tip-tip collision as function of (a) Coulomb interaction parameter, (b) mean fissility, (c) charge asymmetry, (d) mass asymmetry, (d) isospin asymmetry, and (e) charge product when the projectile is spherical ($\beta_{2P} = 0$) and the target is prolate ($\beta_{2T} > 0$).

FIG. 7. Variation of quasifission barrier as function of (a) projectile quadrupole deformation and (b) target quadrupole deformation.

barrier as a function of χ_m is provided by Eq. (6) where $x = \chi_m$. The coefficients are listed in Table I. The effects of quadrupole deformation of projectile and target on quasifission barriers were studied. Figures 7(a) and 7(b) show the plot of quasifission barrier as function of projectile and target quadrupole deformation. The analysis of B_{qf} as a function of β_{2p} shows that there is no systematic variation of quasifission barriers with the projectile's quadrupole deformation. However, a well-organized pattern is observed in the case of target quadrupole deformation. An increase in the quasifission barrier is observed with an increase in quadrupole deformation of the target. The possibility of the formation of compound nuclei will precisely depend on the quasifission barrier. Consequently, the larger quasifission barrier leads to the formation of compound nuclei in sequence with the target's quadrupole deformation factor.

B. Role of angular momentum on quasifission barrier

As an example, the effect on quasifission barrier from angular momentum is presented in Fig. 8 for the fusion reactions ^{58}Fe + ^{244}Pu, ^{50}Ti + ^{252}Cf, and ^{53}V + ^{249}Bk. A large quasifission barrier height is observed for the fusion reaction ^{50}Ti + ^{252}Cf, for which $\eta_A = 0.67$, and smaller in the case of ^{58}Fe + ^{244}Pu ($\eta_A = 0.615$). In each fusion reaction, it is noticed that the value of the quasifission barrier decreases with an increase in angular momentum. The smaller quasifission barrier at higher angular momentum ($\ell = 60\hbar$) decreases the lifetime of formed compound nuclei and vice versa. The figure elucidates the larger quasifission barrier height of about 6.28 MeV in the case of ^{50}Ti + ^{252}Cf at zero angular momentum. Hence, among the studied fusion reactions, a larger probability of the formation of compound nuclei may be observed for ^{50}Ti + ^{252}Cf when compared to the other two fusion reactions. In the subsequent analysis, we studied quasifission barrier height and evaporation residue cross sections. In this regard, among the 90 different fusion reactions studied, we considered the top nine fusion reactions with larger quasifission barrier height. The extracted values of B_{qf} of these fusion reactions are Tabulated in Table II. The production cross sections are predicted using survival probability [51], P_{CN} [52], and P_{xn} using a set of equations available in literature [33]. Γ_n/Γ_f is evaluated using recent studies [53],

TABLE II. Tabulation of fusion reaction, beam intensity (BI), evaporation channel, mass asymmetry, quadrupole deformation of projectile-target nuclei, fusion barrier height, center-of-mass energy, quasifission barrier, and evaporation residue cross sections.

Reaction	BI (pps)	n	η_A	β_{2P}	β_{2T}	V_B (MeV)	E_{cm} (MeV)	B_{qf} (MeV)	σ_{evr} (fb)	Remark
^{50}Ti(stbl.)+^{252}Cf(2.64 yr)	1.135×10^{10}	3	0.67	0	0.236	221.5	223	6.28	49	
^{53}V(1.5 m)+^{249}Bk(330 d)	1.09×10^{10}	3	0.65	0	0.235	240.36	229	5.92	40	Case III
^{54}Cr(stbl.)+^{248}Cm(3.48×10^5 yr)	1.04×10^{10}	3	0.64	0.18	0.235	235.9	236	5.21	34	
^{58}Fe(stbl.)+^{244}Pu(8.13×10^7 yr)	9.6×10^9	3	0.62	0.199	0.224	263.41	249	4.38	38	
^{63}Cu(stbl.)+^{239}Pa(1.8 h)	8.65×10^9	3	0.59	0162	0.224	268.54	260	3.23	19	
^{70}Zn(stbl.)+^{232}Th(stbl.)	8.32×10^9	3	0.57	0.045	0.207	272.34	281	2.93	16	
^{80}Se(stbl.)+^{222}Rn(3.82 d)	7.34×10^9	3	0.47	0.15	0.137	292.97	309	1.39	13	Case II
^{74}Ge(stbl.)+^{228}Ra(5.75 yr)	7.81×10^9	3	0.51	−0.224	0.18	283.41	240	5.63	36	
^{64}Ni(stbl.)+^{238}U(4.46 × 10^9 yr)	8.91×10^9	3	0.57	−0.087	0.215	261.25	267	4.33	30	Case I
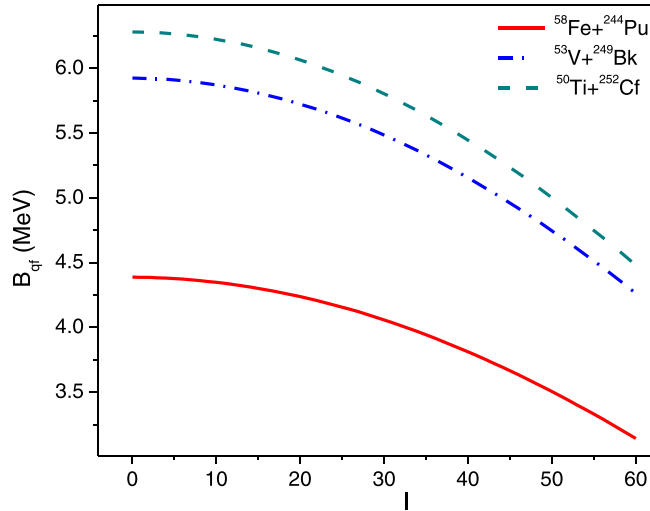
FIG. 8. Variation of quasifission barrier height as a function of angular momentum for the fusion reactions ^{58}Fe $+ ^{244}$Pu (continuous line), ^{50}Ti $+ ^{252}$Cf (dashed line). and ^{53}V $+ ^{249}$Bk (dash-dotted line).

TABLE III. Comparison of evaporation residue cross sections (pb) produced by the present work with that of the predictions of previous reports [59,60] for synthesis of superheavy element $Z = 119$ and 120.

Reaction	E^* (MeV)	σ_{ER} (pb) Refs. [59,60]	PW
^{56}Ti $+ ^{251}$Cf $\rightarrow ^{304}$120 $+ 3n$	36	2.19×10^{-5}	1.37×10^{-5}
^{57}Ti $+ ^{251}$Cf $\rightarrow ^{304}$120 $+ 4n$	47	1.3×10^{-5}	2.56×10^{-5}
^{58}Ti $+ ^{251}$Cf $\rightarrow ^{304}$120 $+ 5n$	60	2.48×10^{-6}	2.0×10^{-6}
^{58}V $+ ^{249}$Bk $\rightarrow ^{304}$120 $+ 3n$	37	1.8×10^{-5}	5.57×10^{-5}
^{59}V $+ ^{249}$Bk $\rightarrow ^{304}$120 $+ 4n$	47	9.96×10^{-6}	2.64×10^{-6}
^{60}V $+ ^{249}$Bk $\rightarrow ^{304}$120 $+ 5n$	59	4.76×10^{-6}	6.73×10^{-6}
^{59}Cr $+ ^{248}$Cm $\rightarrow ^{304}$120 $+ 3n$	36	1.68×10^{-5}	3.31×10^{-5}
^{60}Cr $+ ^{248}$Cm $\rightarrow ^{304}$120 $+ 4n$	46	9.5×10^{-6}	4.32×10^{-6}
^{61}Cr $+ ^{248}$Cm $\rightarrow ^{304}$120 $+ 5n$	57	4.18×10^{-6}	4.18×10^{-6}
^{45}Sc $+ ^{248}$Cf $\rightarrow ^{290}$119 $+ 3n$	39	3.0×10^{-1}	7.15×10^{-1}
^{50}Ti $+ ^{247}$Bk $\rightarrow ^{294}$119 $+ 3n$	36	3×10^{-2}	2.08×10^{-2}
^{51}V $+ ^{242}$Cm $\rightarrow ^{290}$119 $+ 3n$	38	2×10^{-2}	5.0×10^{-2}
^{54}Cr $+ ^{242}$Am $\rightarrow ^{293}$119 $+ 3n$	37	1.5×10^{-3}	3.79×10^{-3}

fission barrier height (B_f) [54], and shell corrections [55]. The excitation-dependent average angular momentum is deduced from Capurro *et al.* [56]. The pairing energy term δP is evaluated using the set of equations given in [57] and $\hbar\omega = 2.2$ MeV [58]. As the mass asymmetry of the fusion reactions decreases, the quasifission barrier height also decreases. The larger B_{qf} of about 6.28 and 5.92 MeV are observed for the reactions induced by the spherical projectiles ^{50}Ti and ^{53}V (case III). Sequentially, production cross sections decrease with decrease in η_A in cases II and I. In addition to detailed investigations, we also compared evaporation residue cross sections (pb) obtained by the present study and those predicted in earlier reports [59,60], as shown in Table III. The different isotopes of projectiles Ti, V, Cr, and Sc on actinide targets were evaluated. The cross sections obtained from the present work show good agreement with the data available in the literature.

IV. CONCLUSIONS

In summary, we have considered 90 different projectile-target combinations for the synthesis of a superheavy element ^{302}120 using the DNS approach. The role of the angle of orientation in quasifission barrier height is studied for both projectile and target nuclei. The quasifission barrier height shows a larger value when an angle of orientation is about 90°, i.e., tip-tip orientation. Further, quasifission barriers are studied for different projectile-target combinations. The role of entrance channel effects—such as Coulomb interaction parameter, mean fissility, charge asymmetry, mass asymmetry, isospin asymmetry, and charge product—on quasifission barriers was investigated. The effect of the deformation parameter on projectile and target nuclei was considered. About 25 projectile-target combinations are recognized with $\beta_{2P} < 0$, $\beta_{2T} > 0$, 50 with $\beta_{2P} > 0$, $\beta_{2T} > 0$, and around 15 with $\beta_{2P} = 0$, $\beta_{2T} > 0$. We have proposed a semiempirical formula for the quasifission barrier as a function of entrance channel parameters. A systematic variation of quasifission barriers with respect to target quadrupole deformation is observed when compared to projectile quadrupole deformation. For fusion reactions with larger quasifission barriers, evaporation residue cross sections were tabulated. Larger B_{qf} is observed for the reactions induced by spherical projectiles such as ^{50}Ti and ^{53}V. Very interestingly, it is observed that the fusion reactions consist of reactions that were used attempting to synthesize the superheavy nuclei $Z = 120$. The predicted evaporation residue cross sections are > 10 fb. A good agreement is also observed between present study with that of previous works. As a result, the current study may be useful in devising corrective procedures for future experimental attempts to synthesize superheavy nuclei $Z = 120$.

[1] C.-C. Sahm, H.-G. Clerc, K.-H. Schmidt, W. Reisdorf, P. Armbruster, F. Heßberger, J. Keller, G. Münzenberg, and D. Vermeulen, Hindrance of fusion in central collisions of heavy, symmetric nuclear systems, Z. Phys. A **319**, 113 (1984).

[2] D. J. Hinde, M. Dasgupta, J. R. Leigh, J. P. Lestone, J. C. Mein, C. R. Morton, J. O. Newton, and H. Timmers, Fusion-Fission versus Quasifission: Effect of Nuclear Orientation, Phys. Rev. Lett. **74**, 1295 (1995).

[3] A. Nasirov, A. Fukushima, Y. Toyoshima, Y. Aritomo, A. Muminov, S. Kalandarov, and R. Utamuratov, The role of orientation of nucleus symmetry axis in fusion dynamics, Nucl. Phys. A **759**, 342 (2005).

[4] G. Fazio, G. Giardina, A. Lamberto, R. Ruggeri, C. Saccá, R. Palamara, A. Muminov, A. Nasirov, U. Yakhshiev, F. Hanappe *et al.*, Formation of heavy and superheavy elements by reactions with massive nuclei, Eur. Phys. J. A **19**, 89 (2004).

[5] N. V. Antonenko, E. A. Cherepanov, A. K. Nasirov, V. P. Permjakov, and V. V. Volkov, Compound nucleus formation in reactions between massive nuclei: Fusion barrier, Phys. Rev. C **51**, 2635 (1995).

[6] G. G. Adamian, N. V. Antonenko, and W. Scheid, Characteristics of quasifission products within the dinuclear system model, Phys. Rev. C **68**, 034601 (2003).

[7] R. Smolańczuk, Production mechanism of superheavy nuclei in cold fusion reactions, Phys. Rev. C **59**, 2634 (1999).

[8] G. G. Adamian, N. V. Antonenko, and W. Scheid, Isotopic trends in the production of superheavy nuclei in cold fusion reactions, Phys. Rev. C **69**, 011601(R) (2004).

[9] Y. T. Oganessian, V. K. Utyonkov, Y. V. Lobanov, F. S. Abdullin, A. N. Polyakov, I. V. Shirokovsky, Y. S. Tsyganov, G. G. Gulbekian, S. L. Bogomolov, B. N. Gikal, A. N. Mezentsev, S. Iliev, V. G. Subbotin, A. M. Sukhov, G. V. Buklanov, K. Subotic, M. G. Itkis, K. J. Moody, J. F. Wild, N. J. Stoyer *et al.*, Synthesis of Superheavy Nuclei in the ^{48}Ca + ^{244}Pu Reaction, Phys. Rev. Lett. **83**, 3154 (1999).

[10] Y. T. Oganessian, V. K. Utyonkov, S. N. Dmitriev, Y. V. Lobanov, M. G. Itkis, A. N. Polyakov, Y. S. Tsyganov, A. N. Mezentsev, A. V. Yeremin, A. A. Voinov, E. A. Sokol, G. G. Gulbekian, S. L. Bogomolov, S. Iliev, V. G. Subbotin, A. M. Sukhov, G. V. Buklanov, S. V. Shishkin, V. I. Chepygin, G. K. Vostokin *et al.*, Synthesis of elements 115 and 113 in the reaction ^{243}Am + ^{48}Ca, Phys. Rev. C **72**, 034611 (2005).

[11] Y. T. Oganessian, V. K. Utyonkov, Y. V. Lobanov, F. S. Abdullin, A. N. Polyakov, I. V. Shirokovsky, Y. S. Tsyganov, G. G. Gulbekian, S. L. Bogomolov, B. N. Gikal, A. N. Mezentsev, S. Iliev, V. G. Subbotin, A. M. Sukhov, O. V. Ivanov, G. V. Buklanov, K. Subotic, M. G. Itkis, K. J. Moody, J. F. Wild *et al.*, Synthesis of superheavy nuclei in the ^{48}Ca + ^{244}Pu reaction: ^{288}114, Phys. Rev. C **62**, 041604(R) (2000).

[12] F. Heßberger, S. Hofmann, D. Ackermann, V. Ninov, M. Leino, G. Münzenberg, S. Saro, A. Lavrentev, A. Popeko, A. Yeremin *et al.*, Decay properties of neutron-deficient isotopes ^{256,257}Db, ^{255}Rf, ^{252,253}Lr, Eur. Phys. J. A **12**, 57 (2001).

[13] J. Hamilton, S. Hofmann, and Y. T. Oganessian, Search for superheavy nuclei, Annu. Rev. Nucl. Part. Sci. **63**, 383 (2013).

[14] F. Li, L. Zhu, Z.-H. Wu, X.-B. Yu, J. Su, and C.-C. Guo, Predictions for the synthesis of superheavy elements $Z = 119$ and 120, Phys. Rev. C **98**, 014618 (2018).

[15] H. Manjunatha and K. Sridhar, A detail investigation on the synthesis of superheavy element $Z = 119$, Phys. Part. Nuclei Lett. **16**, 647 (2019).

[16] H. C. Manjunatha, N. Sowmya, N. Manjunatha, P. S. D. Gupta, L. Seenappa, K. N. Sridhar, G. T, and T. Nandi, Entrance channel dependent hot fusion reactions for superheavy element synthesis, Phys. Rev. C **102**, 064605 (2020).

[17] N. Wang, E. G. Zhao, W. Scheid, and S. G. Zhou, Theoretical study of the synthesis of superheavy nuclei with $z = 119$ and 120 in heavy-ion reactions with trans-uranium targets, Phys. Rev. C **85**, 041601(R) (2012).

[18] L. Zhu, W.-J. Xie, and F.-S. Zhang, Production cross sections of superheavy elements $z = 119$ and 120 in hot fusion reactions, Phys. Rev. C **89**, 024615 (2014).

[19] Z.-H. Liu and J.-D. Bao, Calculation of the evaporation residue cross sections for the synthesis of the superheavy element $Z = 119$ via the ^{50}Ti + ^{249}Bk hot fusion reaction, Phys. Rev. C **84**, 031602(R) (2011).

[20] A. K. Nasirov, G. Mandaglio, G. Giardina, A. Sobiczewski, and A. I. Muminov, Effects of the entrance channel and fission barrier in the synthesis of superheavy element $Z = 120$, Phys. Rev. C **84**, 044612 (2011).

[21] K. N. Sridhar, H. C. Manjunatha, and H. B. Ramalingam, Studies on the synthesis superheavy element $Z = 120$, Nucl. Phys. A **983**, 195 (2019).

[22] H. C. Manjunatha, L. Seenappa, P. S. Damodara Gupta, N. Manjunatha, K. N. Sridhar, N. Sowmya, and T. Nandi, Quasifission and fusion-fission lifetime studies for the superheavy element $Z = 120$, Phys. Rev. C **103**, 024311 (2021).

[23] R. du Rietz, E. Williams, D. J. Hinde, M. Dasgupta, M. Evers, C. J. Lin, D. H. Luong, C. Simenel, and A. Wakhle, Mapping quasifission characteristics and timescales in heavy element formation reactions, Phys. Rev. C **88**, 054618 (2013).

[24] K. Nishio, I. Ikezoe, I. Nishinaka, S. Mitsuoka, K. Hirose, T. Ohtsuki, Y. Watanabe, Y. Aritomo, and S. Hofmann, Evidence for quasifission in the sub-barrier reaction of ^{30}Si + ^{238}U, Phys. Rev. C **82**, 044604 (2010).

[25] A. Wakhle, C. Simenel, D. J. Hinde, M. Dasgupta, M. Evers, D. H. Luong, R. du Rietz, and E. Williams, Interplay between Quantum Shells and Orientation in Quasifission, Phys. Rev. Lett. **113**, 182502 (2014).

[26] K. Nishio, H. Ikezoe, S. Mitsuoka, I. Nishinaka, Y. Nagame, Y. Watanabe, T. Ohtsuki, K. Hirose, and S. Hofmann, Effects of nuclear orientation on the mass distribution of fission fragments in the reaction of ^{36}S + ^{238}U, Phys. Rev. C **77**, 064607 (2008).

[27] K. N. Sridhar, H. C. Manjunatha, and H. B. Ramalingam, Search for possible fusion reactions to synthesize the superheavy element $Z = 121$, Phys. Rev. C **98**, 064605 (2018).

[28] H. C. Manjunatha, K. N. Sridhar, and N. Sowmya, Investigations of the synthesis of the superheavy element $Z = 122$, Phys. Rev. C **98**, 024308 (2018).

[29] H. C. Manjunatha and K. N. Sridhar, A probability of synthesis of the superheavy element $Z = 124$, Eur. Phys. J. A **53**, 1 (2017).

[30] H. C. Manjunatha and K. N. Sridhar, Projectile target combination to synthesis superheavy nuclei $Z = 126$, Nucl. Phys. A **962**, 7 (2017).

[31] H. C. Manjunatha, K. N. Sridhar, and N. Sowmya, Investigations on ^{64}Ni + $_{Z}$An^{A} → $_{Z=104-123}$(SHN)$^{A=250-310}$ reactions, Nucl. Phys. A **987**, 382 (2019).

[32] H. C. Manjunatha, K. N. Sridhar, and H. B. Ramalingam, Synthesis of superheavy elements using ^{50,51}V-induced fusion reactions, Nucl. Phys. A **981**, 17 (2019).

[33] H. C. Manjunatha, L. Seenappa, N. Sowmya, and K. N. Sridhar, Investigations on $^{54-60}$Fe + $^{238-244}$Pu → $^{296-302}$120 fusion reactions, Can. J. Phys. **99**, 16 (2021).

[34] H. C. Manjunatha, P. S. Damodara Gupta, N. Sowmya, L. Seenappa, and N. Manjunatha, Systematics of heavy ion fusion with entrance channel and deformation parameters, Phys. Rev. C **104**, 024622 (2021).

[35] P. S. Gupta, H. C. Manjunatha, and N. Sowmya, Investigations on the synthesis of different isotopes of uranium using fusion reactions, Braz. J. Phys. **51**, 1803 (2021).

[36] G. G. Adamian, N. V. Antonenko, H. Lenske, and L. A. Malov, Predictions of identification and production of new superheavy nuclei with $Z = 119$ and 120, Phys. Rev. C **101**, 034301 (2020).

[37] F. Niu, P.-H. Chen, and Z.-Q. Feng, Systematics on production of superheavy nuclei $Z = 119$–122 in fusion-evaporation reactions, Nucl. Sci. Technol. **32**, 1 (2021).

[38] B. M. Kayumov, O. K. Ganiev, A. K. Nasirov, and G. A. Yuldasheva, Analysis of the fusion mechanism in the synthesis of superheavy element 119 via the ^{54}Cr + ^{243}Am reaction, Phys. Rev. C **105**, 014618 (2022).

[39] G. Adamian, N. Antonenko, and H. Lenske, Estimates of production and structure of nuclei with Z = 119, Nucl. Phys. A **970**, 22 (2018).

[40] G. Adamian and N. Antonenko, Optimal ways to produce heavy and superheavy nuclei, Eur. Phys. J. A **58**, 111 (2022).

[41] L. Zhu and J. Su, Unified description of fusion and multinucleon transfer processes within the dinuclear system model, Phys. Rev. C **104**, 044606 (2021).

[42] Z.-H. Wu, L. Zhu, F. Li, X.-B. Yu, J. Su, and C.-C. Guo, Synthesis of neutron-rich superheavy nuclei with radioactive beams within the dinuclear system model, Phys. Rev. C **97**, 064609 (2018).

[43] V. Y. Denisov and I. Y. Sedykh, Production of super-heavy nuclei in cold fusion reactions, Chin. Phys. C **45**, 044106 (2021).

[44] T. L. Zhao, X. J. Bao, and H. F. Zhang, Improvement of evaporation residual cross sections for superheavy nuclei using a neural network method, Nucl. Phys. A **1027**, 122510 (2022).

[45] S. Soheyli and M. V. Khanlari, Theoretical study of effects of the entrance channel on the relative yield of complete fusion and quasifission in heavy-ion collisions within a dinuclear system approach, Phys. Rev. C **94**, 034615 (2016).

[46] M. V. Khanlari and S. Soheyli, Quasifission and fission rates and their lifetimes in asymmetric reactions forming ^{216}Ra within a dinuclear system approach, Phys. Rev. C **95**, 024617 (2017).

[47] M. Wang, W. Huang, F. G. Kondev, G. Audi, and S. Naimi, The AME 2020 atomic mass evaluation (II). Tables, graphs and references, Chin. Phys. C **45**, 030003 (2021).

[48] R. K. Gupta, M. Balasubramaniam, R. Kumar, N. Singh, M. Manhas, and W. Greiner, Optimum orientations of deformed nuclei for cold synthesis of superheavy elements and the role of higher multipole deformations, J. Phys. G: Nucl. Part. Phys. **31**, 631 (2005).

[49] K. Hagino, Hot fusion reactions with deformed nuclei for synthesis of superheavy nuclei: An extension of the fusion-by-diffusion model, Phys. Rev. C **98**, 014607 (2018).

[50] Z.-Q. Feng, G.-M. Jin, F. Fu, and J.-Q. Li, Production cross sections of superheavy nuclei based on dinuclear system model, Nucl. Phys. A **771**, 50 (2006).

[51] A. S. Zubov, G. G. Adamian, N. V. Antonenko, S. P. Ivanova, and W. Scheid, Survival probability of superheavy nuclei, Phys. Rev. C **65**, 024308 (2002).

[52] W. Loveland, Synthesis of transactinide nuclei using radioactive beams, Phys. Rev. C **76**, 014612 (2007).

[53] N. Sowmya, P. S. Damodara Gupta, H. C. Manjunatha, and T. Nandi, Accurate estimation of the neutron and fission decay widths for hot fusion reactions, Phys. Rev. C **105**, 044605 (2022).

[54] V. I. Zagrebaev, Y. Aritomo, M. G. Itkis, Y. T. Oganessian, and M. Ohta, Synthesis of superheavy nuclei: How accurately can we describe it and calculate the cross sections?, Phys. Rev. C **65**, 014607 (2001).

[55] A. N. Kuzmina, G. G. Adamian, N. V. Antonenko, and W. Scheid, Influence of proton shell closure on production and identification of new superheavy nuclei, Phys. Rev. C **85**, 014319 (2012).

[56] O. A. Capurro, D. E. DiGregorio, S. Gil, D. Abriola, M. di Tada, J. O. Fernandez Niello, A. O. Macchiavelli, G. V. Martí, A. J. Pacheco, J. E. Testoni, D. Tomasi, and I. Urteaga, Average angular momentum in compound nucleus reactions deduced from isomer ratio measurements, Phys. Rev. C **55**, 766 (1997).

[57] P. Möller and J. R. Nix, Nuclear pairing models, Nucl. Phys. A **536**, 20 (1992).

[58] C. Xia, B. Sun, E. Zhao, and S. Zhou, Systematic study of survival probability of excited superheavy nuclei, Science Chin. Phys. Mech. Astron. **54**, 109 (2011).

[59] J.-X. Li and H.-F. Zhang, Predictions for the synthesis of the Z = 120 superheavy element, Phys. Rev. C **106**, 034613 (2022).

[60] J.-X. Li and H.-F. Zhang, Predictions for the synthesis of the Z = 119 superheavy element, Phys. Rev. C **105**, 054606 (2022).